GEOFLUIDS

Geofluids (2009) 9, 237–250 doi: 10.1111/j.1468-8123.2009.00250.x

Response of Alum Rock springs to the October 30, 2007 Alum Rock earthquake and implications for the origin of increased discharge after earthquakes

MICHAEL MANGA[1] AND JOEL C. ROWLAND[2]

[1]*Earth and Planetary Science, University of California, Berkeley, Berkeley, CA, USA;* [2]*Los Alamos National Laboratory, Los Alamos, NM, USA*

ABSTRACT

The origins of increased stream flow and spring discharge following earthquakes have been the subject of controversy, in large part because there are many models to explain observations and few measurements suitable for distinguishing between hypotheses. On October 30, 2007 a magnitude 5.5 earthquake occurred near the Alum Rock springs, California, USA. Within a day we documented a several-fold increase in discharge. Over the following year, we have monitored a gradual return towards pre-earthquake properties, but for the largest springs there appears to be a permanent increase in discharge. The Alum Rock springs discharge waters that are a mixture between modern (shallow) meteoric water and old (deep) connate waters expelled by regional transpression. After the earthquake, there was a small and temporary decrease in the fraction of connate water in the largest springs. Accompanying this geochemical change was a small (1–2°C) temperature decrease. Combined with the rapid response, this implies that the increased discharge has a shallow origin. Increased discharge at these springs occurs both for earthquakes that cause static volumetric expansion and for those that cause contraction, supporting models in which dynamic strains are responsible for the subsurface changes that cause flow to increase. We make a quantitative comparison between the observed changes and model predictions for three types of models: (i) a permanent increase in permeability; (ii) an increase in permeability followed by a gradual decrease to its pre-earthquake value; and (iii) an increase of hydraulic head in the groundwater system discharging at the springs. We show that models in which the permeability of the fracture system feeding the springs increases after the earthquake are in general consistent with the changes in discharge. The postseismic decrease in discharge could either reflect the groundwater system adjusting to the new, higher permeability or a gradual return of permeability to pre-earthquake values; the available data do not allow us to distinguish between these two scenarios. However, the response of these springs to another earthquake will provide critical constraints on the changes that occur in the subsurface and should permit a test of all three types of models.

Key words: connate, earthquake triggering, liquefaction, permeability change, springs, transpression

Received 28 February 2009; accepted 12 May 2009

Corresponding author: Michael Manga, Earth and Planetary Science, University of California, Berkeley, CA, USA. Email: manga@seismo.berkeley.edu. Tel: 1-510-643-8532. Fax: 1-510-643-9980.

Geofluids (2009) 9, 237–250

INTRODUCTION

Increased discharge at springs following regional earthquakes is among the more interesting hydrological responses to earthquakes because the changes are often persistent, can be observed directly, and in some cases are large enough to be visually compelling. Despite a long history of documented changes, the origin of changes in discharge remains uncertain, and has been the subject of some scientific debate (Montgomery & Manga 2003).

There are four general classes of explanations for increased discharge. First, coseismic static strain increases pore pressure in the deformation quadrant that experiences compression (e.g. Wakita 1975; Jonsson *et al.* 2003), leading to increased discharge at the surface (Muir-Wood & King 1993). These static strains may also open or close fractures and hence change permeability. Second, dynamic strains created by the earthquake increase permeability permitting more rapid flow and hence increased discharge (e.g. Briggs 1991; Rojstaczer & Wolf 1992; Curry *et al.*

1994; Rojstaczer *et al.* 1995; Tokunaga 1999; Sato *et al.* 2000; Wang *et al.* 2004a; Charmoille *et al.* 2005). The dynamic strain from distant earthquakes has been shown to at least temporarily increase permeability (e.g. Elkhoury *et al.* 2006). Third, the breaching of hydraulic barriers or seals (e.g. Sibson 1994; Brodsky *et al.* 2003; Wang *et al.* 2004b) is similar to the enhanced permeability model, and the addition of a new water source should be reflected in changes in the composition or temperature of discharged fluids. Fourth, the origin of the excess water discharged after the earthquake lies in the shallowest subsurface where water is liberated by the consolidation or even liquefaction of near-surface unconsolidated materials (e.g. Manga 2001; Manga *et al.* 2003; Montgomery *et al.* 2003).

Here we document the increased discharge and subsequent recovery of a set of thermal springs in San Jose, California, USA in response to the magnitude 5.5 October 30, 2007 Alum Rock earthquake. King *et al.* (1994) have previously reported the response of two of these springs to several regional earthquakes. Our monitoring extends this previous study to one more earthquake. More significantly, we sample water and measure discharge more frequently and consider the response of a greater number of springs. We characterize some of the attributes of earthquakes that have caused responses at the springs. We rule out mechanisms that appeal to coseismic volumetric strain and favor models in which the permeability of the fracture network feeding the springs increases after the earthquake. We test proposed hypotheses and compare mathematical representations of conceptual models of hydraulic head and permeability increases with the observed changes. Finally, we contrast the response of the stream into which the springs discharge with the observed changes at the springs.

SETTING AND PROPERTIES OF THE SPRINGS

The Alum Rock complex of springs consists of a set of thermal springs that discharge from a fracture zone located updip of one strand of the Hayward fault. The springs lie along both sides of the topographic low created by the Penitencia Creek. Figure 1 shows the location of the springs with respect to regional faults.

In a previous study of the hydrogeological and hydrogeochemical features of these springs, Rowland *et al.* (2008) noted significant compositional differences in the water from different springs. The spring water was inferred to be

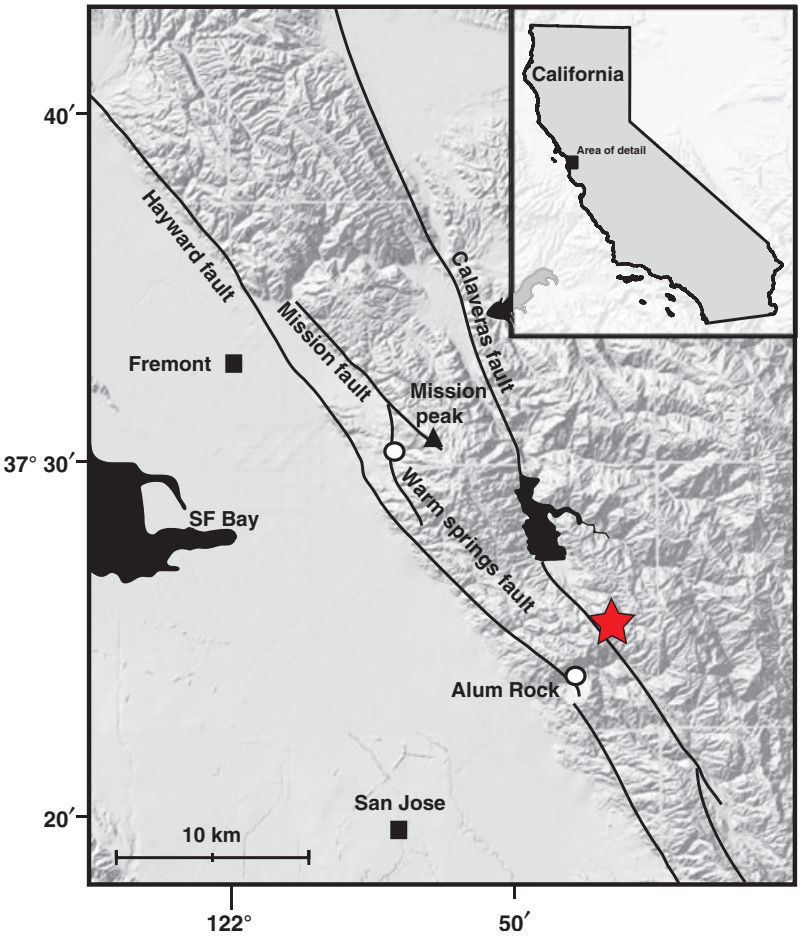

Fig. 1. Location of Alum Rock springs (circle), the 30 October 2007 magnitude 5.5 Alum Rock earthquake (star), and regional faults (black lines). Background is the US Geological Survey 10 m DEM. Fault locations are from Andrews *et al.* (1993).

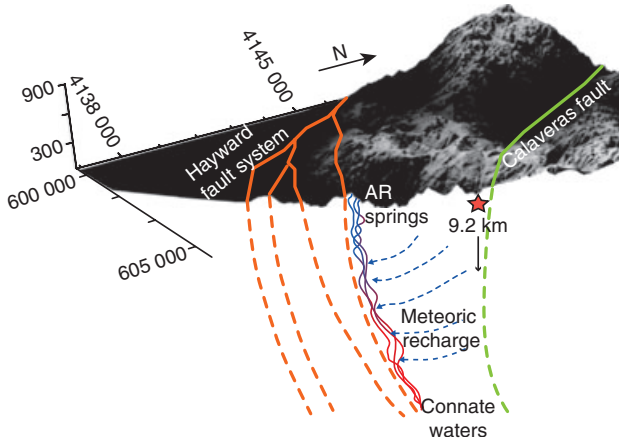

Fig. 2. Conceptual model showing the relationship between faults, flow paths and the sources of deep connate waters and shallow groundwater that has a modern meteoric origin. Location of the Alum Rock earthquake is shown with the star.

Fig. 3. Location of springs along Penitencia Creek. Numbers correspond to spring numbers. DEM source: GeoEarthScope, Northern California LiDAR funded by NSF.

a mixture of locally derived (but tritium free for at least spring AR 4) meteoric water and high chloride water with a pronounced oxygen isotope shift away from meteoric water. The high chloride water was interpreted to be old seawater (a connate water). Given the large variation over small spatial distances, Rowland *et al.* (2008) concluded that the flow paths feeding individual springs remain relatively isolated from each other. Figure 2 illustrates this conceptual model. Because the hydrogeochemistry at the spring outlets depends on the relative contribution of meteoric and connate water (hereafter also called 'shallow' and 'deep', respectively), any earthquake-induced changes in fault-zone permeability or aquifer head should produce changes not only in discharge but potentially also in hydrogeochemistry.

In the 1980s, King *et al.* (1994) documented flow and temperature changes at springs AR 4 and 11 (Fig. 3) following five regional earthquakes. In all cases flow increased, and for a couple of the earthquakes, a small decrease in temperature was recorded. No clear changes in electrical conductivity were recorded, implying that there were no significant hydrogeochemical changes.

On October 30, 2007 at 8:05 PM local time, a magnitude 5.5 earthquake occurred along the Calaveras fault (http://www.earthquake.usgs.gov/). The following morning, we collected water samples and made discharge measurements. We made subsequent measurements over the following year with a sampling frequency that decreased as the earthquake-induced changes decreased. Compared with King *et al.* (1994), we significantly increased the sampling frequency in order to document the evolution of the response; King *et al.* (1994) typically obtained only a single measurement of increased discharge after each earthquake. We documented the responses of 12 springs and Penitencia Creek. Figure 3 shows the locations of these springs relative to each other and Penitencia Creek into which they discharge.

Springs discharge from outlets that range from seeps (AR 2, 5), to small pipes (AR 1, 6, 7, 8, 9, 10 and 13) to large tunnels (springs 4, 11 and 12). Figure 4 shows some of these outlets. Discharge was measured by molding an oil-based modeling clay onto the rocks in order to capture all the spring water and focus it into a bucket for weighing or a graduated cylinder for volume measurement. Uncertainties in discharge are estimated to be about 10%. Meaningful discharge measurements could only be made regularly at springs 4, 6, 11, 12 and 13. At other springs, there were multiple outlets or not enough head to accurately gauge the flow. At some of the springs, water occasionally backed up to form pools which prevented discharge from being measured.

Temperature was measured with a thermocouple with accuracy of 0.2°C until February 2008 and thereafter with a thermistor with accuracy of 0.1°C. O and H isotopes were measured with a GV IsoPrime gas source mass spectrometer, MultiPrep and elemental analyzer (GV Instruments, Wythenshawe, Manchester, UK); analytical precision is approximately 0.1‰ and 1‰ for $\delta^{18}O$ and δD, respectively. Chloride was measured in the laboratory with an ion-specific electrode; uncertainties are estimated to be 10% and are dominated by uncertainty in the calibration and instrument drift between calibration measurements.

From 2003 until the time of the earthquake, we periodically measured discharge and temperature, and collected

Fig. 4. Photographs of AR 12 and AR 11, which emerge from tunnels, Penitencia Creek and travertine mounds which form at the spring outlets.

samples for stable-isotope and major ion measurements. Up to eight stable-isotope samples were analysed at the high-discharge springs (4 and 11) while several of the seeps were only analysed twice. The total number of pre-earthquake flow and temperature measurements varied similarly between springs. Rowland *et al.* (2008) present the results of this monitoring program and discuss the implications of geochemical variations between springs on the connectivity of the fracture network feeding the springs.

RESPONSES

At all spring outlets where we could measure flow, discharge increased following the earthquake. At some of other springs (AR 1, 2), new seeps and outlets formed. At the rest, water backed up in pools because of the increased discharge. Figure 5 shows the flow, temperature and oxygen-isotope response of the two largest springs, AR 4 and 11. These two springs are characterized by a nearly constant temperature (±0.7 and ±1.5°C, respectively). Flow increased by a factor of 3 and 3.5, respectively, within a day of the earthquake. Discharge declined gradually over the subsequent year, but more than 400 days after the earthquake is still above the pre-earthquake discharge: by about 35% for AR 4 and 20% for AR 11. For AR 11, the new steady discharge is similar to the steady discharge in the early 1980s (King *et al.* 1994), whereas pre-earthquake discharge was similar to that measured by King *et al.* (1994) in the early 1990s. At both springs there was a modest decrease in $\delta^{18}O$, 0.2–0.3‰, that occured soon after the earthquake (AR 4) or peaked a few months after the earthquake (AR 11), with a subsequent return to

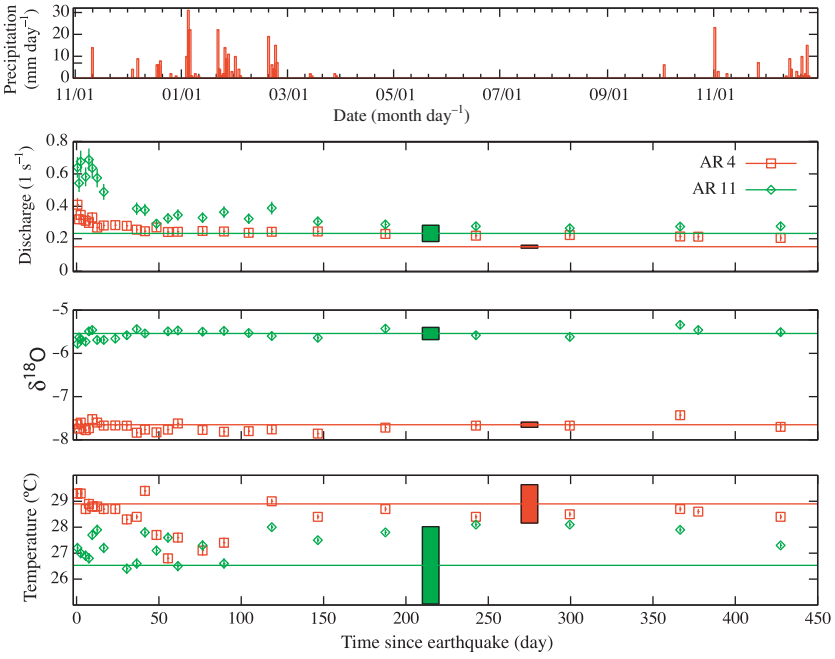

Fig. 5. Discharge, $\delta^{18}O$, and temperature responses at the two largest springs, AR 4 and 11, as a function of time in days since the October 30, 2007 Alum Rock earthquake. Histogram at the top shows precipitation in mm day^{-1}. Horizontal lines are pre-earthquake values and the boxes the standard deviations of pre-earthquake measurements from Rowland *et al.* (2008).

pre-earthquake values. We use $\delta^{18}O$ here to identify changes in water composition, rather than chloride, because we have more pre-earthquake measurements of the former and hence can more reliably compare responses with pre-earthquake values. The decrease in $\delta^{18}O$ appears to be correlated with a small, less than 1–2°C, decrease in temperature.

Measurements at the remaining three springs, AR 6, 12 and 13, for which reliable gauging measurements were made are shown in Fig. 6. These springs differ from AR 4 and 11 in that they showed modest (a few degree) seasonal variations in temperature, presumably because their smaller discharge allows for more heat exchange with the shallow subsurface. The discharge responses at AR 12 and 13 are similar to those at the two largest springs, in that the largest discharges occured within the first few days after the earthquake, but differ in that discharge returned to the pre-earthquake values within a year. AR 6 is different. The first noticeable discharge at what was originally a minor seep appeared 3 days after the earthquake. Subsequently, discharge decreased and the spring returned to a seep within a few months. Measureable discharge returned during late spring 2008 – the rainy season – and again in December 2008. There is no clear change in $\delta^{18}O$ following the earthquake, but we emphasize that for AR 6 we have no pre-earthquake values and for AR 12 and 13 we have only two and five pre-earthquake values, respectively.

Figure 7 shows the relationship between O and H isotope measurements and O isotopes and chloride concentration for all measurements and for all springs. Figure 7 confirms that the water being discharged at the springs resembles a mixture of meteoric waters (low chloride with O and H isotopes close to the meteoric water line) and a high chloride, O isotope shifted water that Rowland *et al.* (2008) inferred to be connate water. The large variations in $\delta^{18}O$ and chloride at springs AR 5, 7 and 9 probably reflect enhanced discharge of shallow groundwater associated with seasonal precipitation.

All springs show small variations over time, possibly related to changes in mixing proportions, but these changes are small compared with the range shown by the entire group of springs. Even springs that showed a compositional response to the earthquake (AR 4 and 11) show no more variation than other springs. Thus, the sudden increase in discharge cannot be attributed to a huge increase in the proportion of any one end-member or some new fluid component not normally present.

FEATURES OF THE EARTHQUAKES THAT CAUSE FLOW TO INCREASE

Table 1 lists the sign of the volumetric strain in the Penitencia Creek drainage basin generated by earthquakes that caused discharge to increase. The list of responses include

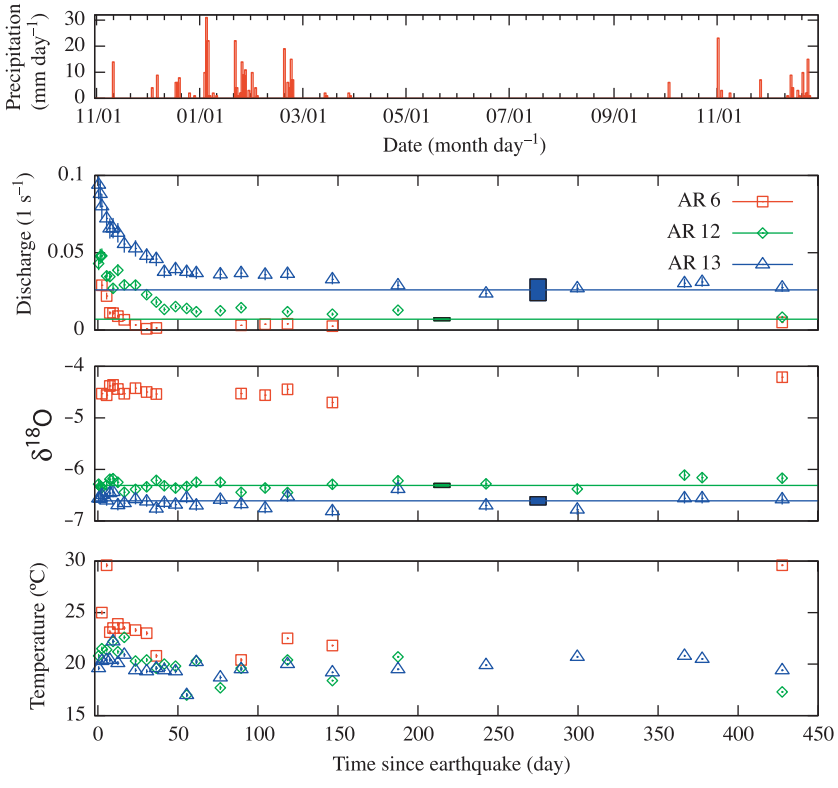

Fig. 6. Discharge, $\delta^{18}O$, and temperature responses at springs AR 6, 12, and 13 as a function of time in days since the October 30, 2007 Alum Rock earthquake. Hyetograph at the top shows precipitation in mm day^{-1}. Horizontal lines are pre-earthquake values and the boxes the standard deviations of pre-earthquake measurements from Rowland *et al.* (2008). Pre-earthquake oxygen isotope values are not known for AR 6 which was a minor seep prior to the earthquake.

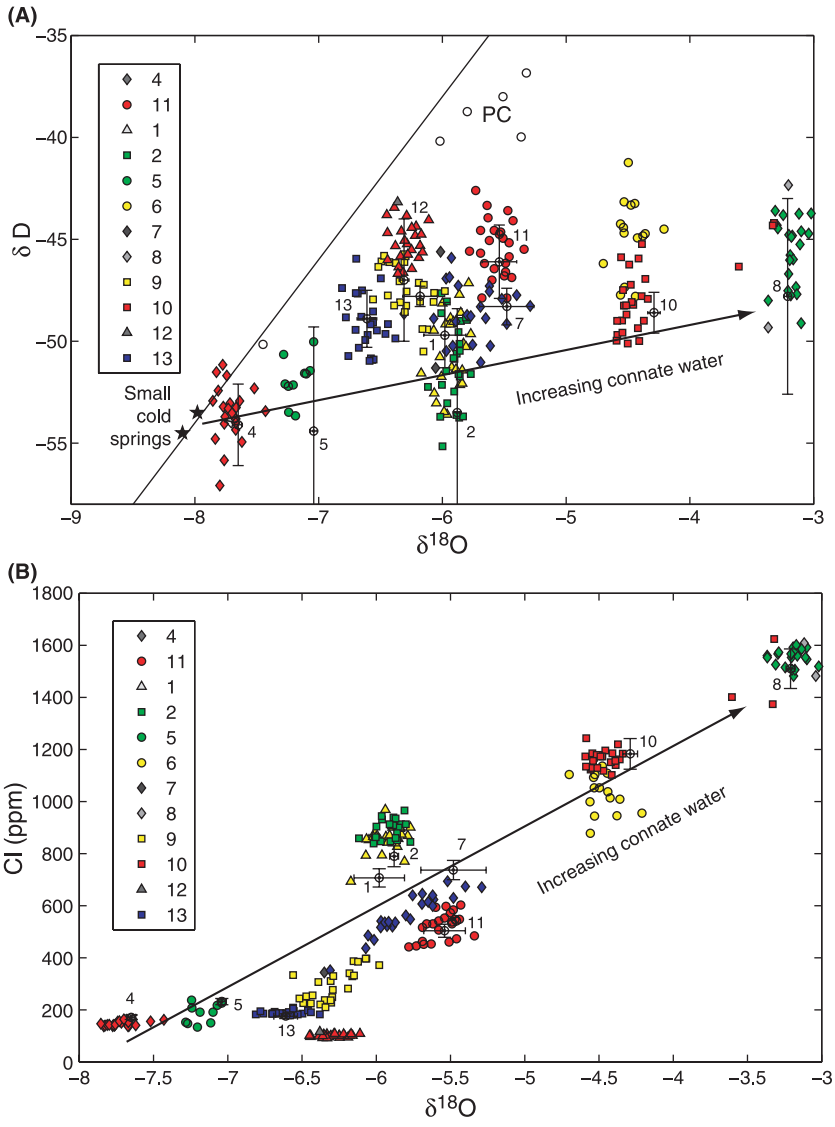

Fig. 7. Relationship between (A) $\delta^{18}O$ and δD and (B) $\delta^{18}O$ and chloride for spring waters collected after the Alum Rock earthquake (colored symbols) and pre-earthquake values (black circles). Error bars on pre-earthquake values reflect the variability in the measurements, summarized and reported by Rowland *et al.* (2008). Uncertainties on any individual measurement are 0.1‰ for $\delta^{18}O$, 1‰ for δD, and 10% for chloride. Error bars are not shown for colored symbols. The two filled stars in (A) are water samples from small springs at high elevations in the drainage basin, the open circles are waters from Penitencia Creek, and the sloping black line is the global meteoric water line $\delta D = 8\delta^{18}O + 10$. There is a pronounced oxygen isotope shift in the spring waters, and (B) shows that this isotope shift is correlated with an enrichment in chloride.

those in King *et al.* (1994), the response to the 2007 Alum Rock earthquake reported here, and a possible response to the 1906 San Francisco earthquake. For the latter we include a question mark in Table 1 because our reading of the Lawson (1908) report left us with some uncertainty about the actual springs being described, though increased discharge was widely reported throughout the area and to distances from the epicenter that exceed that of the Alum Rocks springs. For the 2007 earthquake, the volumetric strain was calculated by Kelly Grijalva (personal communication, 2008) using the deformation formulation in Pollitz (1996), the San Francisco area earth structure model of Dreger & Romanowicz (1994) and a slip model provided by Doug Dreger (personal communication, 2008). The springs lie close to a nodal plane in the pattern of volumetric strain, and peak strains are < 0.2 microstrain. As noted by King *et al.* (1994), discharge at Alum Rock springs increases for earthquakes that cause contraction, expansion or little volumetric strain near the springs. Subsurface changes that increase flow are thus probably dominated by dynamic stresses.

Figure 8 shows the relationship between distance of the earthquake from the springs, earthquake magnitude and the response of the springs. Earthquake locations and magnitudes are derived from the Northern California Earthquake Data Center. There is a clear magnitude–distance relationship for causing discharge to increase. However, we are unable to identify whether this is a true threshold because we do not have access to reliable measurements of the magnitude of increased discharge for events prior to the 2007 Alum Rock earthquake. That is, we cannot determine whether the magnitude of the discharge increase scales with the magnitude of earthquake-induced strains (e.g. peak ground velocity), as found for

Table 1. Earthquakes followed by flow increases.

Date	Event	Magnitude	Epicentral distance	Volumetric strain*	Reference
4/18/1906?	San Francisco	7.8	70 km	D	Lawson (1908)?
4/24/1984	Morgan Hill	6.2	18 km	C	King *et al.* (1994)
3/31/1986	Mount Lewis	5.7	15 km	C	King *et al.* (1994)
6/13/1988	Alum Rock	5.3	8 km	C	King *et al.* (1994)
4/3/1989	Alum Rock	4.5	5 km	–	King *et al.* (1994)
10/18/1989	Loma Prieta	7.0	40 km	D	King *et al.* (1994)
10/30/2007	Alum Rock	5.5	4 km	–	This study

*C, D and '–' indicate contraction, dilatation, or that the basin is close to a nodal plane in the strain, respectively.

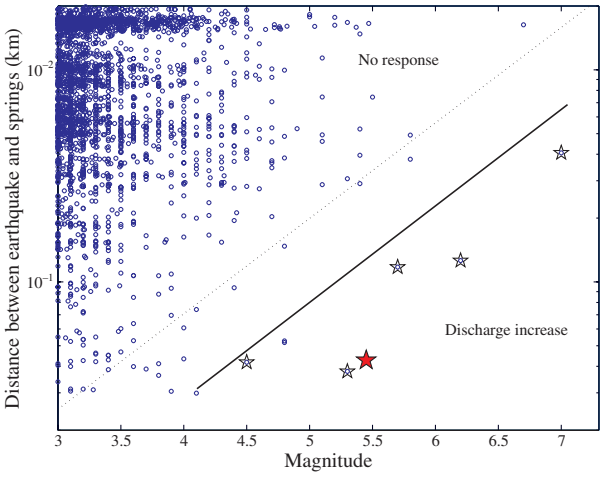

Fig. 8. Magnitude and distance from the springs of earthquakes that occurred during the period monitored: 1977–1991 by King *et al.* (1994), and 2003–December 31, 2008 (Rowland *et al.* 2008 and present study). Red stars indicate earthquakes for which discharge increased; the filled-in star is the October 30, 2007 Alum Rock earthquake. Open blue circles are earthquakes for which there is no (documented) change in discharge. The sloping dotted line is an empirical magnitude–distance threshold for changes in streamflow based on a global compilation (Wang *et al.* 2006); while empirical this line corresponds to a line of approximately constant seismic energy density (Wang 2007). The solid line is an empirically drawn line that separates earthquakes that caused discharge changes from those that did not and has a similar slope to that for the global compilation.

permeability changes in wells (Elkhoury *et al.* 2006). Nevertheless, we draw an empirical threshold separating earthquakes that have caused flow to increase from those that did not. Over the cumulative period that was monitored, 1977–1991 and 2003–2008, there are no events clearly beyond this threshold line for which flow did not increase. Two earthquakes lie very close to the threshold (magnitude 4.8 events on January 15, 1981 and November 10, 1988); both caused contraction in the Alum Rock region. The interval between earthquakes that caused a response is as short as 6.5 months so that if there is a repose or recovery time required for an earthquake-induced response it is less than half a year. A repose time of a couple of years was identified for other earthquake-triggered phenomena, including mud volcanoes in Azerbaijan (Mellors *et al.* 2007), Japan (Manga *et al.* 2009) and Italy (Bonini 2009).

DISCUSSION

We begin by listing features of the observations reported in the previous two sections that have a bearing on the origins and implications of the spring response.

(1) Discharge increased at all springs.

(2) Peak discharge occurred soon after the earthquake, within a few days.

(3) Discharge does not always return to pre-earthquake values, most notably at the two largest springs where we also have the best constraints on pre-earthquake discharges.

(4) While discharge increased by factors exceeding 3, the isotopic composition and chloride concentration changed modestly, if at all. For the two largest springs there was a small deviation towards the meteoric end-member composition. The observation of small if any change is consistent with the absence of any electrical conductivity changes reported by King *et al.* (1994) following previous earthquakes. Changes in $\delta^{18}O$ and chloride plot along a mixing line between meteoric and connate water end-members (Fig. 7), supporting the conceptual model (Fig. 2) in which these sources of water mix to varying degrees.

(5) There is a clear magnitude–distance relationship for earthquakes that induce responses (Fig. 8).

(6) For the largest springs there was a small decrease in temperature (<1–2°C) that occurs at the same time as changes in $\delta^{18}O$. We did not observe the immediate and small (approximately 1°C) temperature decrease reported by King *et al.* (1994).

(7) The response is dominated by dynamic rather than static stress changes (Table 1).

Table 2 summarizes some of the predictions of proposed models for the increase in discharge after earthquakes. Observations 1 and 4 support models in which permeability increases at shallow depths or within the fracture system feeding the springs; changes at depth would result in a delayed response. Observation 4 shows that we do not need to appeal to a new source of fluid or chemistry from a breached reservoir (e.g. Sibson 1994; Wang *et al.* 2004b), a coseismic and postseismic feature that has been documented at springs elsewhere (e.g. Yechieli & Bein 2002; Stejskal *et al.* 2008). Given the small decrease in temperature at the largest

Table 2. Model and expected changes at the springs.

Model	Prediction for the springs
Coseismic elastic strain	Temperature increase; larger fraction of 'deep' water; correlation with sign of volumetric strain
Enhanced permeability	Temperature and composition changes will depend on where the changes occur; potential for permanent changes in flow and composition
Ruptured subsurface reservoirs and fault valves	Increased temperature; semi-permanent to permanent change in discharge and composition, with more 'deep' water or new water component
Consolidation/liquefaction	Decreased temperature; larger fraction of shallow water; eventual return to pre-earthquake properties

springs (AR 4 and 11) and that the discharged water at AR 4 contains no ^{3}H (Rowland *et al.* 2008), a vadose zone source for all the excess water (e.g. Manga *et al.* 2003) is highly unlikely (but see the section about the response of Penitencia Creek). Because of observation 4, we will next consider models only for changes in discharge, and address the changes of hydrogeochemistry qualitatively. Observation 7 is counter to predictions of the coseismic elastic strain model.

Figure 9 illustrates three conceptual models to explain the discharge change. We first consider the model in Fig. 9A which appeals to an increase in permeability of the fracture systems feeding the springs. Second, we consider the model in Fig. 9B in which permeability of the fracture system increases after the earthquake and then gradually reduces over time scales similar to those over which discharge changes. Third, we consider the model in Fig. 9C in which an influx of fluid increases the head in the fracture system. We treat the fracture zone that delivers water to the spring as a homogenous one-dimensional aquifer. While clearly a great oversimplification of what must be a much more complex subsurface, similar (one-dimensional) models are commonly used to interpret postseismic responses to earthquakes (e.g. Rojstaczer *et al.* 1995; Roeloffs 1998; Tokunaga 1999; Sato *et al.* 2000; Manga 2001; Manga *et al.* 2003; Montgomery *et al.* 2003; Wang *et al.* 2004a,b) as well as to interpret discharge variations at springs (e.g. Manga 1996). We will see that, while simple, the models fit the observed changes in discharge extremely well.

Enhanced permeability model

Discharge Q from the fracture zone is governed by Darcy's equation

$$Q = -K_v A \frac{\partial h}{\partial z} \quad \text{at } z = 0, \tag{1}$$

where K_v is the vertical hydraulic conductivity of the fracture zone, A is the cross-sectional area across which fluid is being discharged, z is the depth and h the hydraulic head. Equation (1) implies that the coseismic change in hydraulic conductivity is proportional to the coseismic change in discharge. We refer to a model in which hydraulic conductivity increases as the 'enhanced permeability' model.

Subsequently, the increased discharge leads to a reduction of the head in the fracture system and a greater recharge from the surroundings. Approximating this latter flux as being proportional to the head difference between the far-field h_0 and that in the fracture system, the evolution of head in the fracture system can be approximated by the standard groundwater flow equation with an additional term that accounts for recharge to the fracture zone,

$$S_s \frac{\partial h}{\partial t} = K_v \frac{\partial^2 h}{\partial z^2} + \frac{K_h}{wD}(h_0 - h) \tag{2}$$

with boundary conditions

$$h = h_0 \text{ at } x = D \quad \text{and} \quad \partial h/\partial z = 0 \text{ at } z = L. \tag{3}$$

Here S_s is the specific storage of the fracture zone, the width and depth of the fracture zone are w and L, respectively, and K_h is the horizontal conductivity of the region adjacent to the fracture zone. The horizontal aquifer extends to a distance $x = D$ where the head is fixed to h_0. The last term in equation (2) that describes recharge is a first-order approximation. In this model we assume that storage properties, S_s, do not change, though both hydraulic conductivity and storage properties can be influenced by earthquakes (e.g. Jang *et al.* 2008).

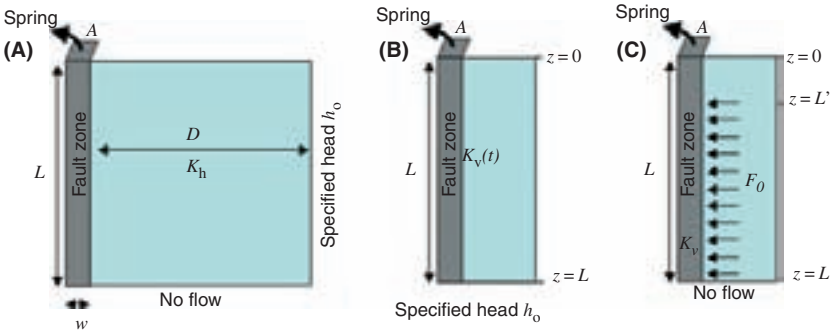

Fig. 9. Schematic illustration of conceptual models. (A) Enhanced permeability model in which the vertical hydraulic conductivity of the fracture zone, K_v, changes after the earthquake. (B) Transient permeability model in which the vertical hydraulic conductivity of the fracture zone, K_v, increases co-seismically and then decreases. (C) Increased head model in which an influx of fluid F_0 causes the head in the fracture zone to increase and hence discharge to increase.

The steady-state head distribution in the fracture zone is

$$h = h_0\left(1 - \frac{\sinh(\mu z) + \sinh[\mu(2L - z)]}{\sinh(2\mu L)}\right) \quad (4)$$

where $\mu = \sqrt{K_h/K_v Dw}$. The corresponding steady-state discharge is

$$Q_0 = K_v A \mu h_0 \left[\frac{1 - \cosh(2\mu L)}{\sinh(2\mu L)}\right]. \quad (5)$$

Following the earthquake, we assume that K_v increases by an amount linearly proportional to the increase in discharge. The subsequent evolution of discharge can be obtained by solving the time-dependent diffusion equation (2) with a new hydraulic conductivity K_{vf} and an initial condition equal to the difference between the steady-state solution with the initial conductivity (now denoted K_{vi}) and final conductivity K_{vf}. The solution can be obtained by adapting that for an analogous problem in section 4.14 of Carslaw & Jaeger (1959). The evolution of head is then given by

$$\begin{aligned} h(z,t) = {} & h_0\left[1 - \frac{\sinh(\mu_f z) + \sinh[\mu_f(2L - z)]}{\sinh(2\mu_f L)}\right] \\ & - \frac{16 h_0 L^2}{\pi} e^{-K_h t/DwS_s} \\ & \sum_{n=1}^{\infty}\left[\frac{\mu_i^2}{(2n-1)^2\pi^2 + 4L^2\mu_i^2} - \frac{\mu_f^2}{(2n-1)^2\pi^2 + 4L^2\mu_f^2}\right] \\ & \times \frac{1}{(2n-1)} \sin\left[\frac{(2n-1)\pi z}{2L}\right] e^{-(2n-1)^2\pi^2 K_{vf} t/4S_s L^2} \end{aligned} \quad (6)$$

where the subscripts 'i' and 'f' indicate values before (initial) and after (final) the earthquake. The corresponding discharge can be obtained by evaluating Darcy's equation (1) at $z = 0$,

$$\begin{aligned} Q(t) = {} & -K_{vf} A \mu_f h_0 \frac{[1 - \cosh(2\mu_f L)]}{\sinh(2\mu_f L)} + 8 K_{vf} A h_0 L e^{-K_h t/DwS_s} \\ & \sum_{n=1}^{\infty}\left[\frac{\mu_i^2}{(2n-1)^2\pi^2 + 4L^2\mu_i^2} - \frac{\mu_f^2}{(2n-1)^2\pi^2 + 4L^2\mu_f^2}\right] \\ & e^{-(2n-1)^2\pi^2 K_{vf} t/4S_s L^2} \end{aligned} \quad (7)$$

This model is similar to that used by Rojstaczer *et al.* (1995) and later invoked by Sato *et al.* (2000) and Tokunaga (1999) to explain changes in discharge. It differs in that it accounts for the increased recharge to the fracture system following its reduction in head, the last term in equation (2).

This enhanced permeability model is characterized by four parameters

$$\alpha = \frac{K_{vf} A h_0}{L}; \quad R = \frac{K_{vf}}{K_{vi}}; \quad \nu = \frac{K_h}{DwS_s}; \quad T = \sqrt{\frac{\nu L^2 S_s}{K_{vf}}} \quad (8)$$

The first, α, is a scaling parameter for the magnitude of discharge. The second, R, is the ratio of fracture-zone conductivity after and before the earthquake. R can be determining directly from the measured increased in discharge. The third, ν, is an inverse hydraulic diffusion time scale. The fourth, T, is the ratio of vertical to horizontal flow time scales. With these parameters, equation (7) can be written

$$\begin{aligned} Q(t) = {} & -\alpha T \frac{[1 - \cosh 2T]}{\sinh 2T} + 8\alpha e^{-\nu t} \\ & \sum_{n=1}^{\infty}\left[\frac{RT^2}{(2n-1)^2\pi^2 + 4RT^2} - \frac{T^2}{(2n-1)^2\pi^2 + 4T^2}\right] \\ & e^{-(2n-1)^2\pi^2\nu t/4T^2} \end{aligned} \quad (9)$$

The ratio of final postearthquake steady-state discharge Q_f to the pre-earthquake discharge Q_0 is

$$\frac{Q_f}{Q_0} = \sqrt{R}\frac{\sinh(2\sqrt{R}T)}{\sinh(2T)}\left(\frac{1 - \cosh 2T}{1 - \cosh 2\sqrt{R}T}\right) \quad (10)$$

From equation (10) we can see that for small T, $Q_f/Q_0 \to 1$, whereas for large T, $Q_f/Q_0 \to \sqrt{R}$. Thus, the initial response to a conductivity increase is an increase in discharge by a factor of R, and the final steady discharge is increased by a factor $\leq \sqrt{R}$.

Transient permeability model

The increase in permeability potentially created by the earthquake may not be permanent as biogeochemical processes will act to decrease the permeability over time (Elkhoury *et al.* 2006). Gradual changes in flow, hydrogeochemistry, or fluid pressure following earthquakes have been attributed to a gradual reduction of earthquake-enhanced permeability (e.g. Gratier *et al.* 2003; Claesson *et al.* 2004, 2007). This model differs from the enhanced permeability model in that K_v is assumed to change on time scales comparable with those over which flow changes. Hereafter we refer to this model as the 'transient permeability model'.

We will assume that hydraulic conductivity increases coseismically from K_{vi} to K_{vf}, as in the enhanced permeability model. Subsequently, we assume K_{vf} decreases exponentially in time with decay constant λ, i.e.

$$K_v(t) = K_{vi} + (K_{vf} - K_{vi})e^{-\lambda t}$$

The choice of an exponential dependence for $K_v(t)$, while arbitrary and unknown *a priori*, is inspired by the exponential time dependence of many geochemical and mechanical processes.

With the boundary condition $h = h_0$ at $z = L$, discharge is then given by equation (1),

$$Q(t) = \frac{K_{vi} A h_0}{l}[1 + (R-1)e^{-\lambda t}] \quad (11)$$

This model is characterized by three parameters

$$Q_0 = \frac{K_{vi} A h_0}{l}; \quad R = \frac{K_{vf}}{K_{vi}}; \quad \lambda. \quad (12)$$

Q_0 is measured and R is known from the magnitude of the increase in discharge leaving us with a single parameter to fit.

Increased head model

If K_v remains unchanged by the earthquake, and assuming A does not change, Darcy's law (1) requires that head gradients, and hence head, changed. Increased stream discharge owing to increased hydraulic heads have been proposed to result from consolidation (e.g. Manga *et al.* 2003), breaching barriers to release pressurized water (Wang *et al.* 2004b) or by increasing permeability perpendicular to the fracture system so that the fracture zone is rapidly recharged (Wang *et al.* 2004a).

Here we follow the formulation in Wang *et al.* (2004a) and allow a pulse of recharge to the fracture system over the depth interval $z = L'$ to $z = L$. The groundwater flow equation for this problem can be written as

$$S_s \frac{\partial h}{\partial t} = K_v \frac{\partial^2 h}{\partial z^2} + F \quad (13)$$

where F is the rate of recharge to the fracture zone per unit volume. At the time of the earthquake we let $F = F_0\delta$ over the depth interval $L' < z < L$, where $\delta = 1$ at $t = 0$ and $\delta = 0$ for $t > 0$. The solution for discharge is given by (e.g. Wang *et al.* 2004a,b)

$$Q(t) = Q_0 + \frac{2K_v A F_0}{S_s L}\sum_{n=1}^{\infty}(-1)^{n-1}\sin\left[\frac{(2n-1)^2\pi^2(L-L')}{2L}\right] \times e^{-(2n-1)^2\pi^2 K_v t/4S_s L^2} \quad (14)$$

This model is characterized by four parameters

$$Q_0; \quad \beta = \frac{2K_v A F_0}{S_s L}; \quad \Lambda = \frac{K_v}{S_s L^2}; \quad (L-L')/L. \quad (15)$$

Of these, the discharge Q_0 prior to the earthquake is known. We will fix $(L - L')/L$ to 1 in order to reduce the number of parameters. This choice is consistent with the very rapid increase in discharge – as $(L - L')/L$ decreases, the time between the earthquake and the peak postseismic discharge increases. Previous studies that documented peak responses within days inferred $(L - L')/L$ close to 1 (Manga *et al.* 2003; Wang *et al.* 2004a) and these studies guide our simplification.

Application of models to the flow observations

We determined model parameters and their uncertainties by fitting equations (9), (11) and (14) to the discharge measurements using the nonlinear least-squares Marquardt-Levenberg algorithm (see chapter 15.5 in Press *et al.* 1992). The misfit between the best-fit model and data is characterized with the root mean squared deviation

$$E = \left[\frac{1}{N}\sum_{i=1}^{N}(Q_{\text{measured}} - Q_{\text{model}})^2\right]^{1/2}$$

where N is the number of discharge measurements.

Figure 10 compares data for AR 4, 6, 11, 12 and 13 with best-fit models. Tables 3, 4 and 5 list the model parameters. The larger uncertainties in the parameters of the enhanced permeability model (Table 3) compared with the increased head model (Table 5) reflect the larger number of fitted parameters (3 compared with 2) and the trade-offs between their values.

In general, the enhanced permeability model, equation (9), captures the recovery of the discharge after the earthquake. Importantly, this model can also explain the permanent change in discharge measured at springs AR 4 and 11. The magnitude of the long-term change in discharge depends on the conductivity change R and ratio of time scales T (equation 10). If the evolution of discharge is dominated by a time evolution of permeability, then the final permeability in the transient permeability model must be different from its pre-earthquake value for springs 4 and 11 (observation 3 in the list at the beginning of this section). The transient permeability model, if the correct model, implies permeability reduction times of between about 10 and 30 days ($1/\lambda$). The increased head model also captures the postseismic increase and subsequent decrease of discharge, but requires a return to pre-earthquake discharge Q_0. The values of ν and T for the enhanced permeability model, or Λ in the increased head model, correspond to reasonable hydraulic diffusivities of $O(10^{-1})$ m^2 s^{-1} (e.g. Roeloffs 1996) if we assume a length scale L of 1 km.

We do not attempt to use the misfit between model and data, represented by E in Tables 3–5, to make a quantitative decision about which model best explains the postseismic changes. For the largest springs, AR 4 and 11, the enhanced permeability model clearly fits the data better, the larger number of model parameters notwithstanding. However, as we do not know the functional form for possible sealing of fractures and permeability reduction, we cannot dismiss the transient permeability model.

Given the small changes in water hydrogeochemistry at the largest springs we do not quantitatively apply the models in Fig. 9 to the hydrogeochemistry data. We note, however, that the essentially constant water composition

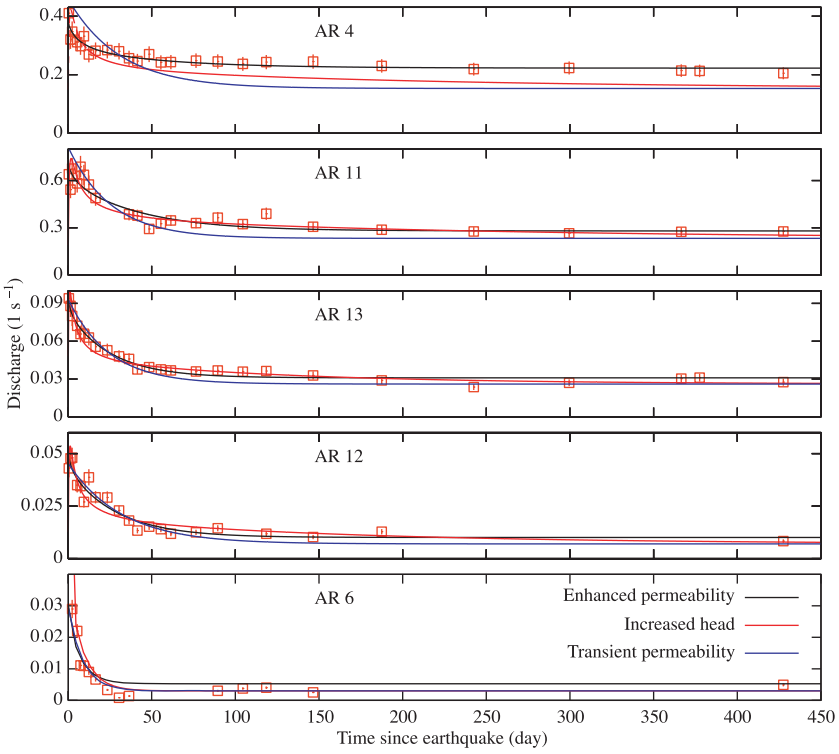

Fig. 10. Comparison of discharge measurements (symbols) with best fit models for the 5 springs for which reliable discharge measurements could be made. Black, red and blue curves are the enhanced permeability, increased head, and transient permeability models, respectively, with model parameters listed in Tables 3–5.

Table 3 Model parameters for enhanced permeability model.

Spring	R^*	α (l s^{-1})	T	ν (day^{-1})	E (l s^{-1})
AR 4	3.0	0.14 ± 0.02	1.7 ± 0.2	0.0093 ± 0.0030	0.017
AR 11	3.5	0.66 ± 0.18	0.70 ± 0.14	0.0039 ± 0.0018	0.057
AR 13	3.6	0.19 ± 0.05	0.42 ± 0.06	0.0025 ± 0.0007	0.0032
AR 12	6.5	0.076 ± 0.047	0.37 ± 0.15	0.0018 ± 0.0016	0.0037
AR 6	10	0.012 ± 0.01	0.1*	0.00056 ± 0.00007	0.0047

*Fixed to this value.

Table 4 Model parameters for transient permeability model.

Spring	Q_0*	R^*	λ (day^{-1})	E (l s^{-1})
AR 4	0.153	3.0	0.034 ± 0.007	0.071
AR 11	0.233	3.5	0.041 ± 0.007	0.093
AR 13	0.026	3.6	0.042 ± 0.004	0.0040
AR 12	0.007	6.5	0.033 ± 0.003	0.011
AR 6	0.003	10	0.11 ± 0.02	0.0031

*Fixed to this value.

Table 5 Model parameters for increased head model.

Spring	Q_0* (l s^{-1})	β (l s^{-1})	Λ (day^{-1})	E (l s^{-1})
AR 4	0.153	0.072 ± 0.007	0.0050 ± 0.0010	0.050
AR 11	0.233	0.14 ± 0.01	0.0044 ± 0.0007	0.073
AR 13	0.026	0.0205 ± 0.0007	0.0081 ± 0.0007	0.0046
AR 12	0.007	0.0127 ± 0.0006	0.062 ± 0.0007	0.0043
AR 6	0	0.035 ± 0.004	0.115 ± 0.020	0.0017

*Fixed to this value.

may imply a long residence time of water in the fracture system compared to the period over which discharge changes. Otherwise the water entering the fracture system should be evident as a dilution of the chloride concentration and decrease in $\delta^{18}O$. Whereas discharge increased by a factor of 3–7 for the springs shown in Figs 5 and 6, the water is diluted by at most a few percent by the shallow meteoric end-member. For the enhanced permeability model (Fig. 9A), springs AR 4 and 11 have the largest value of T – that is, they are the springs for which horizontal flow times are shortest relative to vertical flow times – and also show the most pronounced dilution of discharged water, as expected. Finally, if the fracture system was draining water from two distinct regions, an increase in fracture zone permeability would increase the proportion of water being recharged from the deeper region, presumably our chloride-rich end-member. If the enhanced permeability model is in fact a good description of the subsurface, then the shallow and deep water must mix upgradient and before the mixture is drawn into the fracture system where the permeability increased.

RESPONSE OF PENITENCIA CREEK

Penitencia Creek also responded to the earthquake by increasing its discharge. The Santa Clara Valley Water District maintains a gauge 4 km downstream of the springs, formerly USGS station 11172100. Measurements 8 and 16 h after the earthquake show an approximate doubling

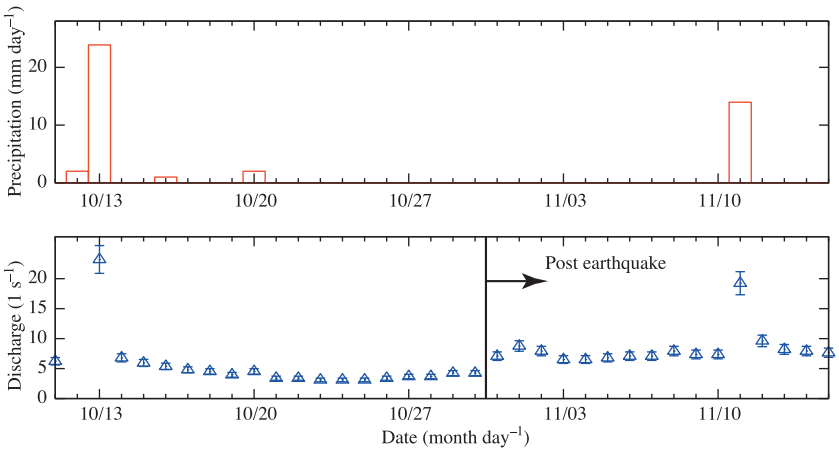

Fig. 11. Discharge in Penitencia Creek and precipitation before and after the October 30, 2007 Alum Rock earthquake. Discharge approximately doubled after the earthquake and remained elevated until precipitation on November 11 obscures any earthquake induced changes.

of the discharge from about 4 to 8 l s^{-1}. Figure 11 shows that the increased discharge persists for at least 12 days until rainfall on November 11 adds ambiguity to interpreting subsequent discharge measurements. Uncertainity in discharge, based on the accuracy of the water level gauge, is about 10%. The increase in discharge is much greater than the total discharge at the Alum Rock springs (less than 2 l s^{-1} on October 31, 2007) implying a source for some of the excess discharge other than the springs. As with the springs, the peak increased discharge occurred within a couple of days of the earthquake.

We did not collect water from Penitencia Creek until November 5, 2007. Water samples from the creek were collected upstream of all the springs. The samples from November 5 and 7 are unusual compared with all the other creek samples collected both before and since in two respects, as shown in Fig. 12. First, their O and H isotopic composition fall off the trend defined by the other water samples. Second, the chloride concentrations are the highest of any creek samples.

We suggest two possible explanations for the chloride enrichment and isotope shift. First, deep groundwater was released from unidentified springs and seeps upstream of the Alum Rocks springs. This would impart both an oxygen and chloride shift similar to that seen at the Alum Rock springs.

Second, we appeal to a source of water in the shallowest subsurface, where water can experience significant evaporation and transpiration in the vadose zone prior to entering the stream. A chloride enrichment of about 50% over typical values for stream water would imply that one-third of the original water was lost relative to typical streamwater. In an atmosphere with 20% humidity, evaporation of 10% of the water would have imparted a shift in O and H that would bring the original water close to a line described by other streamflow samples (we use the fractionation factors of Cappa *et al.* (2003) at 20°C at 20.4% humidity in this representative calculation). The remaining water loss to

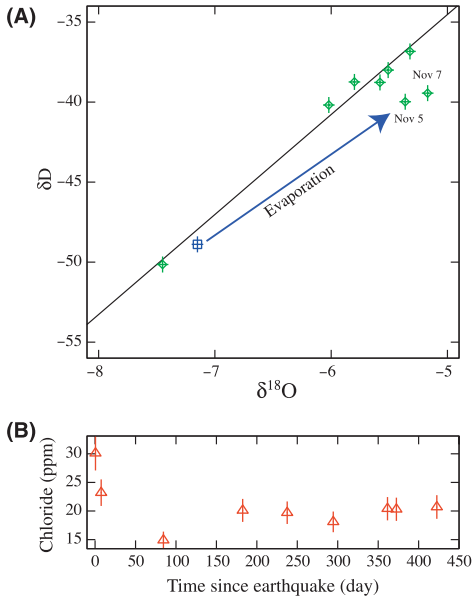

Fig. 12. (A) Oxygen and hydrogen isotope composition of water collected from Penitencia Creek upstream of the springs and after the earthquake (green symbols). The black line is a best-fit to the measurements and has a slope of 6.3, lower than that of the global meteoric water line. The two outliers were the first samples collected after the earthquake, on November 5 and 7, 2007. The blue symbol shows an estimate of water composition from which the November 5 sample could be derived by assuming 10% evaporation at 20°C and 20% humidity. (B) Chloride time series showing that the highest chloride concentration measured in creek water to date were in the first 2 weeks after the earthquake.

account for the 50% enrichment in chloride could be lost by transpiration, as water uptake by roots imparts no fractionation (Gat 1996). November 5, 2007 was near the beginning of the wet season and before any significant rainfall (only one significant storm, on October 13, occurred prior to the earthquake) so soil water should have experienced significant evapotranspiration. In fact, most of the water samples from the dry season lie on a trend that deviates from the meteoric water line by having a more

shallow slope, but none deviate as much as the Novemer 5 and 7, 2007 samples. We suggest that shaking by the earthquake liberated this water, perhaps by consolidating loose materials (Manga *et al.* 2003), and that this water entered the stream. Unfortunately, as no water samples from the creek were collected during the first 5 days after the earthquake, we must view this hydrogeochemically based inference as highly speculative as it is based on two water samples.

The recession of stream discharge after the earthquake offers an additional opportunity to distinguish between explanations for the increased discharge. During periods without significant precipitation, discharge Q will decrease approximately exponentially with time t,

$$Q(t) \propto e^{-\alpha t}. \quad (16)$$

The recession constant α is proportional to the permeability of the aquifers providing baseflow. For the recession from October 14–19 following the storm on October 13, $\alpha = 0.105 \pm 0.005$ day^{-1}; for the period after the earthquake, November 1–5, $\alpha = 0.078 \pm 0.026$ day^{-1}; following the storm on November 11, $\alpha = 0.077 \pm 0.022$ day^{-1} for the period November 12–15. These time intervals are selected because there is no precipitation to confound the analysis. There is no clear change in recession characteristics, consistent with models in which the earthquake increases head in the aquifers providing baseflow (e.g. Manga 2001; Manga *et al.* 2003; Wang *et al.* 2004a). However, we once again emphasize the limited time interval over which the effect of the earthquake can be seen before precipitation obscures the response. In addition, a small reservoir (1.2×10^5 m^3 capacity) in the upper reaches of the Penitencia Creek drainage has an unknown, but likely very small, effect on the discharge at the gauge.

CONCLUSIONS

The Alum Rock springs all showed a rapid postseismic increase in discharge followed by a gradual recovery. The large change in discharge was accompanied by either small or no significant changes in water composition. The small shift towards a composition more similar to meteoric water and the rapid response imply that the excess water originates from shallow depths and that changes occur close to the surface. This does not mean that deep changes do not occur, simply that deep changes do not dominate the observed responses. The lack of correlation between increased discharge and the sign of volumetric strain favors a response induced by dynamic strain.

We briefly considered three different models to explain the flow changes. We favor the model in which permeability increased in the fracture zone feeding the springs over a model in which fluid pressures increased because of the permanent (over a 1-year time window) change in the steady discharge – a feature that requires a permanent change in properties or boundary conditions. Nevertheless, the increased head model and transient permeability models also fit the data quite well.

We should ultimately be able to distinguish between the three models for the evolution of discharge by documenting the response to yet another earthquake. In particular, the recession characteristics of discharge depend on the permeability change for the enhanced permeability model in Fig. 9A. Recession will be identical for all earthquakes for the head-change model in Fig. 9B (Manga 2001), that is, Λ will be the same. If the response to a subsequent earthquake shows a different recession parameter (different Λ), and a recession that does not scale with the permeability increase as described in equation (9), we would favor recession being dominated by time-evolving reduction of permeability. Unfortunately, the long interval between discharge measurements made by King *et al.* (1994) prevents us from performing these tests retrospectively. Furthermore, unlike streams where we can use baseflow recession before and after earthquakes to identify changes (e.g. Manga 2001; Montgomery *et al.* 2003), the normal state of the springs is a steady discharge so that we have (so far) only a single recession event to probe the subsurface changes.

ACKNOWLEDGEMENTS

We thank Alum Rock Park for providing sampling permits; NSF EAR 0909701 for support to respond to the earthquake, NASA for support in making measurements prior to the earthquake, and the Miller Institute for Basic Research in Science for supporting the analysis presented here; the many colleagues, students and in particular family members who assisted with sampling; Tim Rose for ideas and geochemical analyses; Wenbo Yang for the O and H isotope measurements; Linda Kalnejas for help with ion chromatography measurements; Kelly Grivalja for calculating strain; the Santa Clara water district and staff for maintaining the Penitencia Creek gauge and making corrected data available; Chi Wang, Steve Ingebritsen, Bill Evans, Stuart Rojstaczer and an anonymous reviewer for useful suggestions. Model fitting was performed using gnuplot (http://www.gnuplot.info/).

REFERENCES

Andrews DJ, Oppenheimer DH, Lienkamper JJ (1993) The missing link between the Hayward and Calaveras faults. *Journal of Geophysical Research*, **98**, 12,083–95.

Bonini M (2009) Mud volcano eruptions and earthquakes in the Apennines, Italy. *Tectonophysics*. (in press).

Briggs RO (1991) Effects of Loma Prieta earthquake on surface water in Waddell Valley. *Water Resources Bulletin*, **27**, 991–9.

Brodsky EE, Roeloffs E, Woodcock D, Gall I, Manga M (2003) A mechanism for sustained ground water pressure changes induced by distant earthquakes. *Journal of Geophysical Research*, **108** doi: 10.1029/2002JB002321.

Cappa CD, Hendricks MB, DePaolo, DJ, Cohen RC (2003) Isotopic fractionation of water during evaporation. *Journal of Geophysical Research*, **108**, 4525, doi: 10.1029/2003JD003597.

Carslaw HS, Jaeger JC (1959) *Conduction of Heat in Solids*, 2nd edn, Oxford University Press, New York.

Charmoille A, Fabbri O, Mudry J, Guglielmi Y, Bertrand C (2005) Post-seismic permeability change in a shallow fractured aquifer following a M-L 5.1 earthquake (Fourbanne karst aquifer, Jura outermost thrust unit, eastern France). *Geophysical Research Letters*, **32**, L18406, doi: 10.1029/2005GL023859.

Claesson L, Skelton A, Graham C, Dietl C, Morth M, Torssander P, Kockum I (2004) Hydrogeochemical changes before and after a major earthquake. *Geology*, **32**, 641–4.

Claesson L, Skelton A, Graham C, Morth CM (2007) The timescale and mechanisms of fault sealing and water-rock interaction after an earthquake. *Geofluids*, **7**, 427–40.

Curry RR, Emery BA, Kidwell TG (1994) Sources and magnitudes of increased streamflow in the Santa Cruz Mountains for the 1990 water year after the earthquake. *US Geological Survey Professional Paper*, **1551E**, 31–50.

Dreger D, Romanowicz B (1994), Source characteristics of events in the San Francisco Bay Region. *US Geological Survey Open File Report*, **94-176**, 301–9.

Elkhoury JE, Brodsky EE, Agnew DC (2006) Seismic waves increase permeability. *Nature*, **441**, 1135–8.

Gat JR (1996) Oxygen and hydrogen isotopes in the hydrologic cycle. *Annual Reviews of Earth and Planetary Science*, **24**, 225–62.

Gratier JP, Favreau P, Renard F (2003) Modeling fluid transfer along California faults when integrating pressure solution crack sealing and compaction processes. *Journal of Geophysical Research*, **108**, 2104.

Jang CS, Liu CW, Chia Y, Cheng LH, Chen YC (2008) Changes in hydrogeological properties of the River Choushui allunvial fan aquifer due to the 1999 Chi-Chi earthquake, Taiwan. *Hydrogeology Journal*, **16**, 389–97.

Jonsson S, Segall P, Pedersen R, Bjornsson G (2003) Post-earthquake ground movements correlated to pore-pressure transients. *Nature*, **424**, 179–83.

King C-Y, Basler D, Presser TS, Evans WC, White LD, Minissale A (1994) In search of earthquake-related hydrologic and chemical changes along Hayward Fault. *Applied Geochemistry*, **9**, 83–91.

Lawson AC (1908) *The California Earthquake of April 18, 1906*, vol. 1. Report of the State Earthquake Investigation Commission, Carnegie Institution of Washington, Washington, D.C.

Manga M (1996) Hydrology of spring-dominated streams in the Oregon Cascades. *Water Resources Research*, **32**, 2435–9.

Manga M (2001) Origin of postseismic streamflow changes inferred from baseflow recession and magnitude-distance relations. *Geophysical Research Letters*, **28**, 2133–6.

Manga M, Brodsky EE, Boone M (2003) Response of streamflow to multiple earthquakes and implications for the origin of postseismic discharge changes. *Geophysical Research Letters*, **30**.doi: 10.1029/2002GL016618.

Manga M, Brumm M, Rudolph ML (2009) Earthquake triggering of mud volcanos: a review. *Marine and Petroleum Geology*, in press. doi: 10.1016/j.marpetgeo.2009.01.019.

Mellors R, Kilb D, Aliyev A, Gasanov A, Yetirmishli G (2007) Correlations between earthquakes and large mud volcano eruptions. *Journal of Geophysical Research*, **112**, B034304, doi: 101029/2006JB004489.

Montgomery DR, Manga M (2003) Streamflow and water well responses to earthquakes. *Science*, **300**, 2047–49.

Montgomery DR, Greenberg HM, Smith DT (2003) Streamflow response to the Nisqually earthquake. *Earth and Planetary Science Letters*, **209**, 19–28.

Muir-Wood R, King GCP (1993) Hydrological signatures of earthquake strain. *Journal of Geophysical Research*, **98**, 22,035–68.

Pollitz FF (1996) Coseismic deformation from earthquake faulting on a layered spherical earth. *Geophysical Journal International*, **125**, 1–14.

Press WH, Teukolsky SA, Vetterling WT, Flannery BP (1992) *Numerical Recipes: The Art of Scientific Computing*, 2nd edn. Cambridge University Press, New York.

Roeloffs EA (1996) Poroelastic techniques in the study of earthquake-related hydrologic phenomena. *Advances in Geophysics*, **37**, 135–95.

Roeloffs EA (1998) Persistent water level changes in a well near Parkfield, California, due to local and distant earthquakes. *Journal of Geophysical Research*, **103**, 869–89.

Rojstaczer S, Wolf S (1992) Permeability changes associated with large earthquakes: an example from Loma Prieta, California. *Geology*, **20**, 211–14.

Rojstaczer S, Wolf S, Michel R (1995) Permeability enhancement in the shallow crust as a cause of earthquake-induced hydrological changes. *Nature*, **373**, 237–9.

Rowland JC, Manga M, Rose TP (2008) The influence of poorly interconnected fault zone flow paths on spring geochemistry. *Geofluids*, **8**, 93–101.

Sato T, Sakai R, Furuya K, Kodama T (2000) Coseismic spring flow changes associated with the 1995 Kobe earthquake. *Geophysical Research Letters*, **27**, 1219–22.

Sibson RH (1994) Crustal stress, faulting and fluid flow. *Geological Society of London, Special Publication*, **78**, 69–84.

Stejskal V, Malek J, Novotny O (2008) Variations in discharge and temperature of mineral springs at the Frantiskovy Lazne Spa, Czech Republic, duing a nearby earthquake swarm. *Studia Geophysica eet Geodaetica*, **52**, 589–606.

Tokunaga T (1999) Modeling of earthquake-induced hydrological changes and possible permeability enhancement due to 17 January 1995 Kobe earthquake Japan. *Journal of Hydrology*, **223**, 221–9.

Wakita H (1975) Water wells as possible indicators of tectonic strain. *Science*, **189**, 553–55.

Wang C-Y (2007) Liquefaction beyond the near field. *Seismological Research Letters*, **78**, 512–7.

Wang C-Y, Wang C-H, Manga M (2004a) Coseismic release of water from mountains: evidence from the 1999 (Mw = 7.5) Chi-Chi, Taiwan, earthquake. *Geology*, **32**, 769–72.

Wang C-Y, Dreger D, Manga D, Wong A (2004b) Streamflow increase due to rupturing of hydrothermal reservoirs: evidence from the 2003 San Simeon, California, earthquake. *Geophysical Research Letters*, **31**, L10502, doi: 10.1029/2004GL020124.

Wang C-Y, Wong A, Dreger DS, Manga M (2006) Liquefaction limit during earthquakes and underground explosions: implications on ground-motion attenuation. *Bulletin Seismological Society America*, **96**, 355–63.

Yechieli Y, Bein A (2002) Response of groundwater systems in the Dead Sea Rift Valley to the Nuweiba earthquake: changes in head, water chemistry, and near-surface effects. *Journal of Geophysical Research*, **107**, 2332, doi: 10.1029/2001JB001100.